Electro-Optic Frequency Beam Splitters and Tritters for High-Fidelity Photonic Quantum Information Processing

Hsuan-Hao Lu,[1] Joseph M. Lukens,[2] Nicholas A. Peters,[2,3] Ogaga D. Odele,[1] Daniel E. Leaird,[1]
Andrew M. Weiner,[1] and Pavel Lougovski[2,*]

[1]*School of Electrical and Computer Engineering and Purdue Quantum Center,*
Purdue University, West Lafayette, Indiana 47907, USA
[2]*Quantum Information Science Group, Computational Sciences and Engineering Division,*
Oak Ridge National Laboratory, Oak Ridge, Tennessee 37831, USA
[3]*Bredesen Center for Interdisciplinary Research and Graduate Education,*
The University of Tennessee, Knoxville, Tennessee 37996, USA

We report the experimental realization of high-fidelity photonic quantum gates for frequency-encoded qubits and qutrits based on electro-optic modulation and Fourier-transform pulse shaping. Our frequency version of the Hadamard gate offers near-unity fidelity (0.99998 ± 0.00003), requires only a single microwave drive tone for near-ideal performance, functions across the entire C band (1530–1570 nm), and can operate concurrently on multiple qubits spaced as tightly as four frequency modes apart, with no observable degradation in the fidelity. For qutrits, we implement a 3×3 extension of the Hadamard gate: the balanced tritter. This tritter—the first ever demonstrated for frequency modes—attains fidelity 0.9989 ± 0.0004. These gates represent important building blocks toward scalable, high-fidelity quantum information processing based on frequency encoding.

Introduction.—The coherent translation of quantum states from one frequency to another via optical non-linearities has been the focus of considerable research since the early 1990s [1]; yet only fairly recently have such processes been explored in the more elaborate context of time-frequency quantum information processing (QIP), where the optical frequency is not just the *carrier* of quantum information but the *information itself*. Important examples include the quantum pulse gate [2,3], which uses nonlinear mixing with shaped classical pulses for selective conversion of the time-frequency modes of single photons [4–6], and demonstrations of frequency beam splitters based on both $\chi^{(2)}$ [7,8] and $\chi^{(3)}$ [9–11] nonlinearities, which interfere two wavelength modes analogously to a spatial beam splitter. These seminal experiments have shown key primitives in frequency-based QIP, but many challenges remain. For example, optical filters and/or low temperatures are required to remove background noise due to powerful optical pumps, from either the sources themselves or Raman scattering in the nonlinear medium. And achieving the necessary nonlinear mixing for arbitrary combinations of modes will require additional pump fields, as well as properly engineered phase-matching conditions.

Recently, we proposed a fundamentally distinct platform for frequency-bin manipulations, relying on electro-optic phase modulation and Fourier-transform pulse shaping for universal QIP [12]. Our approach requires no optical pump fields, is readily parallelized, and scales well with the number of modes. In this Letter, we apply this paradigm to experimentally demonstrate the first electro-optic-based frequency beam splitter. Our frequency beam splitter attains a high fidelity, operates in parallel on multiple two-mode subsets across the entire optical C band, and retains excellent performance at the single-photon level. Moreover, by incorporating an additional harmonic in the microwave drive signal, we also realize a balanced frequency tritter, the three-mode extension of the beam splitter. This is the first frequency tritter demonstrated on any platform and establishes our electro-optic approach as a leader for high-dimensional frequency-based QIP. Combined with its native parallelizability and absence of optical noise sources, our mixer design offers new opportunities for a range of quantum information applications, including linear-optical computation [12], quantum repeaters [13], and quantum walks [14]. The tritter also serves as an elementary building block for a frequency version of three-mode directionally unbiased linear-optical multiports, which find application in quantum simulations [15] and Bell state discriminators [16].

Background.—The Hilbert space of interest consists of a comb of equispaced frequency bins, with operators $\hat{a}_n$ ($n \in \mathbb{Z}$) that annihilate a single photon in the narrow-band modes centered at frequencies $\omega_n = \omega_0 + n\Delta\omega$ [12,17]. A qudit is represented by a single photon spread over d such modes, and the objective is to implement a frequency multiport V connecting the input $\hat{a}_n^{(\text{in})}$ and output $\hat{a}_m^{(\text{out})}$

modes in some desired fashion: $\hat{a}_m^{(\text{out})} = \sum_n V_{mn} \hat{a}_n^{(\text{in})}$. Line-by-line pulse shaping [18,19] permits arbitrary phase shifts for frequency modes, i.e., the operation $V_{mn} = e^{i\phi_m}\delta_{mn}$. Following the initial demonstration of entangled-photon temporal shaping in 2005 [20], a range of experiments have showcased the utility of pulse shaping at the single-photon level [21–25].

However, universal QIP also requires frequency mode *mixing*. And while, as noted above, parametric processes have enabled two-mode frequency beam splitters, electro-optic modulation represents an attractive alternative: It requires no optical pumps, relies on purely electrical controls, and is compatible with state-of-the-art telecommunication technology. Such features have enabled impressive electro-optic experiments in quantum photonics, including single-photon temporal shaping [26–30], nonlocal modulation cancellation [17,31,32], and state measurement [33,34]. Nevertheless, the realization of an arbitrary $d \times d$ frequency-bin multiport presents stark challenges for a single electro-optic phase modulator (EOM). By design, an EOM couples a single input frequency mode to many output modes, unavoidably scattering an input photon outside of the d-dimensional computational space. A simple argument suggests that this undesired "scatter probability" is at least $(d-1)/(2d-1)$ for a uniform d-mode mixer based on a single EOM [35]. Yet this limitation can be circumvented by considering two EOMs with a pulse shaper sandwiched between them; the spectral phase imparted by the middle stage ensures that the sidebands populated after the first EOM are returned to the computational space after the second one, thereby making it possible to realize a fully deterministic frequency beam splitter [12].

Quantitatively, the performance of a generic frequency multiport V can be compared to the desired $d \times d$ unitary operation $U_{d \times d}$ through success probability $\mathcal{P} = (1/d)\text{Tr}(V_{d \times d}^\dagger V_{d \times d})$ and fidelity $\mathcal{F} = (1/\mathcal{P}d^2)|\text{Tr}(V_{d \times d}^\dagger U_{d \times d})|^2$ metrics, where $V_{d \times d}$ denotes the infinite-dimensional unitary V truncated to the d modes of $U_{d \times d}$ [35,36]. Experimentally, the success probability is further degraded by photon loss, an effect absent in an ideal unitary. But since insertion loss is distinct from operation purity—the former being technical in nature, and the latter stemming from fundamental properties of the modulation approach—we normalize the measured linear transformation by total transmissivity before computing $\mathcal{P}$.

Frequency beam splitter.—For our first experimental demonstration, we focus on the 50/50 beam splitter with phases chosen to match the Hadamard gate:

$$U_{2 \times 2} = \frac{1}{\sqrt{2}}\begin{pmatrix} 1 & 1 \\ 1 & -1 \end{pmatrix}, \qquad (1)$$

the top row corresponding to mode 0 (ω_0) and the bottom to mode 1 (ω_1). We make use of two improvements from our original solution in Ref. [12], which result in a more practical experimental setup. First, we can absorb the initial
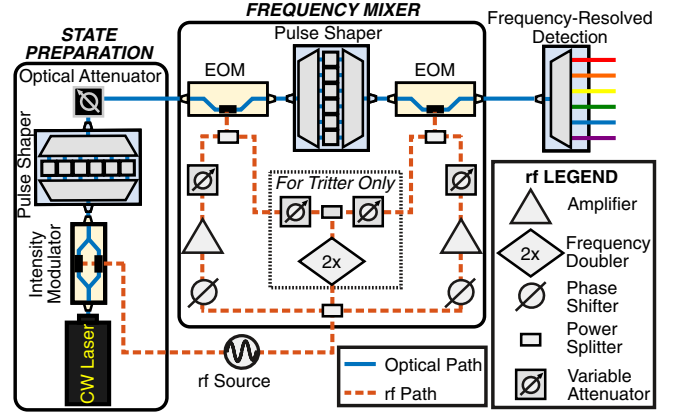

FIG. 1. Experimental setup. See the text and Ref. [35] for details.

pulse shaper into the first EOM, thereby reducing the number of optical components from four to three; second, by considering only phase-shifted sine waves as the electro-optic modulation functions—rather than arbitrary waveforms—the theory still predicts $\mathcal{F} = 0.9999$ and $\mathcal{P} = 0.9760$ [35]: a small reduction from unity and well above the single-EOM limit of $\mathcal{P} = 2/3$. This near-ideal performance even with such a simple microwave modulation represents a major theoretical advance in terms of practicality and scalability, removing the need for a high-bandwidth arbitrary waveform generator to realize the Hadamard gate. Moreover, while we focus on nearest-neighbor mode coupling, in which the microwave drive frequency equals the fundamental mode spacing $\Delta\omega$, spectrally separated modes can be mixed as well. Setting the modulation frequency to an integer multiple $N\Delta\omega$ produces a frequency beam splitter for lines now spaced N modes apart, all while avoiding cross talk with interior modes, assuming a pure $N\Delta\omega$-periodic drive. Using the pulse-shaper phases, it is then even possible to realize different operations on these interleaved N-harmonic "supergrids," potentially permitting an array of independent nearest-neighbor and nonadjacent frequency operations within the same set of elements.

Figure 1 provides a schematic of the experimental setup [35]. A radio-frequency (rf) oscillator provides a 25-GHz drive signal to each EOM, with amplifiers and delay lines setting the appropriate amplitude and phase for each waveform. The central pulse shaper applies the numerically optimized spectral phase pattern for the Hadamard gate. The $\sim$10-GHz spectral resolution of this pulse shaper ultimately limits the tightest frequency-mode spacing (and thus total number of modes) we can utilize in our setup; experimentally we have found a detectable reduction in $\mathcal{F}$ and $\mathcal{P}$ for spacings below $\sim$18 GHz. To characterize the full frequency-bin multiport, we probe it with an electro-optic frequency comb, measuring the output spectrum for different input frequency superpositions. This technique represents
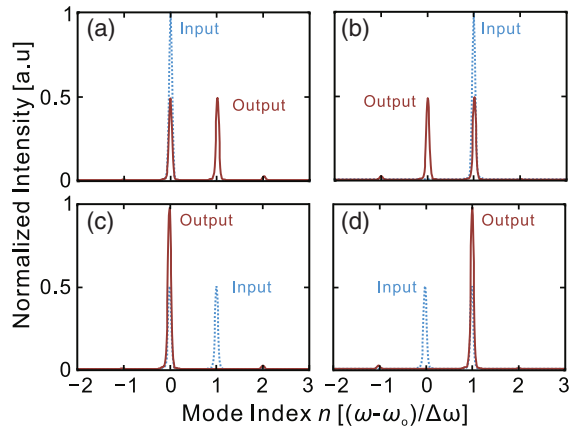
FIG. 2. Experimentally measured beam splitter output spectra for specific coherent state inputs. (a) Pure mode 0, $|\alpha_{\omega_0} 0_{\omega_1}\rangle$. (b) Pure mode 1, $|0_{\omega_0} \alpha_{\omega_1}\rangle$. (c) Mode 0 and mode 1 in phase, $|\alpha_{\omega_0} \alpha_{\omega_1}\rangle$. (d) Mode 0 and mode 1 out of phase, $|\alpha_{\omega_0} (-\alpha)_{\omega_1}\rangle$.
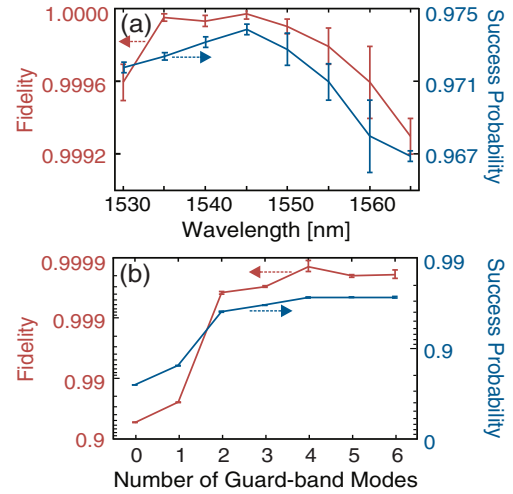

FIG. 3. (a) Fidelity and success probability as a function of the center wavelength. (b) Parallel beam splitter performance against frequency separation.

the analogue of the spatial version proposed and demonstrated in Ref. [37], applied here for the first time to frequency modes [35]. We also adopt the convention [37] which specifies zero phase as the input superposition state that maximizes the power in the zeroth frequency bin of the output; the phase values of any subsequent state (as set by the state preparation pulse shaper in Fig. 1) are thus defined only relative to this operating point. At a center wavelength of 1545.04 nm ($\omega_0 = 2\pi \times 194.036$ THz), we measure fidelity $\mathcal{F} = 0.99998 \pm 0.00003$ and success probability $\mathcal{P} = 0.9739 \pm 0.0003$, where error bars give the standard deviation of five independent measurement sequences. The current gate insertion loss is 12.5 dB: The EOMs contribute ∼2.8 dB each; the pulse shaper ∼4.7 dB; and the remainder comes from fiber patch cord connections and polarization controllers.

Figure 2 shows four experimentally recorded input-output combinations: The top row shows the equiamplitude superpositions resulting from input in either mode 0 or mode 1; the second row reveals the single-wavelength output with the input in the states $|\alpha_{\omega_0} (\pm\alpha)_{\omega_1}\rangle$. The small bumps in adjacent modes −1 and +2 reflect the nonunity success probability, a limitation which—as noted above—could be removed by more sophisticated modulation waveforms. And even in the current arrangement with $\mathcal{P} \approx 0.97$, the impact such residual scattering could have on gates downstream—i.e., by coupling back into the computational space and introducing errors—can be eliminated, either by using the next pulse shaper to selectively attenuate these modes or by sending them to a fiber tap for detection.

A crucial claim in favor of our beam splitter is its suitability for parallelization. Ironically, the very characteristic which precludes a deterministic frequency beam splitter using a single EOM—frequency-translation invariance [35]—enables nearly effortless parallelization. After properly compensating dispersion across the optical

spectrum (to synchronize group delay between the two EOMs), we scan the wavelength of the central gate mode in 5-nm increments and measure $\mathcal{F}$ and $\mathcal{P}$ at each step over the full C band. Figure 3(a) shows that the fidelity exceeds 0.9990 for all test points, and the success probability does not drop below 0.965. A second question, complementary to the total acceptance bandwidth, is the minimum frequency spacing: How close can two single-qubit gates be placed without performance degradation? Since sidebands adjacent to the computational space are populated mid-calculation, one would expect that a finite number of dark, guard-band modes are required to prevent cross-contamination. We address this question experimentally by implementing two beam splitters in parallel and characterizing the total operation as a function of the number of initially empty modes between mode 1 of the low-frequency gate and mode 0 of the higher-frequency one. The fidelity and success probability for the collective parallel operation are plotted in Fig. 3(b); they reach their asymptotic values for separations of just four modes. Combined with the 40-nm (5-THz) bandwidth of Fig. 3(a) and the 25-GHz mode spacing, these results imply that the present system can realize 33 frequency beam splitters in parallel—a remarkable indication of the promise of our approach in scalable QIP.

Frequency tritter.—Thus far, quantum frequency mixers have focused on the basic two-mode case [7–11], yet the inherent high dimensionality of frequency-bin states makes them well suited for more complex qudit operations as well. Accordingly, generalizing mode mixers to dimensions beyond $d = 2$ represents an important milestone for frequency-based QIP. For $d = 3$, the most natural operation is the uniform frequency tritter—the frequency analogue of a 3×3 spatial coupler with equal split ratios [38], which has been shown to enable fundamentally richer quantum

physics than the two-mode case [39]. The specificity of such an operation distinguishes the frequency tritter from previous examples of frequency conversion which, while involving three distinct modes, have not attained arbitrary control over the full 3×3 interaction [40]. For our purposes, a particularly convenient operation satisfying the equiamplitude requirement is the three-point discrete Fourier transform:

$$U_{3\times3} = \frac{1}{\sqrt{3}} \begin{pmatrix} 1 & 1 & 1 \\ 1 & e^{2\pi i/3} & e^{4\pi i/3} \\ 1 & e^{4\pi i/3} & e^{2\pi i/3} \end{pmatrix}. \qquad (2)$$

Numerically, we find that incorporating an additional harmonic in the EOM drive signals allows our current configuration to reproduce the above frequency tritter with predicted fidelity $\mathcal{F} = 0.9999$ and success probability $\mathcal{P} = 0.9733$ [35]. The fact that the modulation remains so simple even for the tritter operation—consisting of the sum of just two phase-shifted sine waves—again manifests the fortuitous practicality of our Fourier-series approach, beyond even the original proposal which relied on specialized rf waveforms [12].

Experimentally, we incorporate a rf frequency doubler into the setup (see the dotted box in Fig. 1) to produce the necessary second harmonic. Because of the high-frequency rolloff of our microwave components, we also reduce the drive frequency—and, hence, mode spacing—from 25 to 18.1 GHz, for a doubled component at 36.2 GHz [41]. Running the coherent-state-based characterization algorithm [35,37], we measure fidelity $\mathcal{F} = 0.9989 \pm 0.0004$ and success probability $\mathcal{P} = 0.9730 \pm 0.0002$, again extremely close to the theoretical predictions. Figure 4 plots several important input-output spectra: For any single-line input, the output exhibits equal lines in the same three
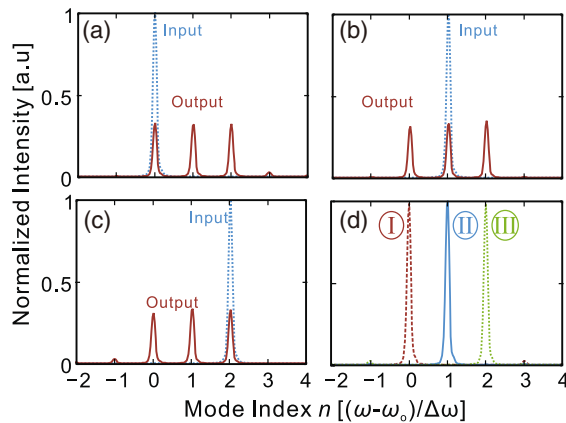
modes; conversely, three-mode input superpositions of the appropriate phases excite single lines at the output. This high-fidelity, balanced frequency tritter—the first of its kind—confirms that our electro-optic technique scales well to higher dimensions, with only a minor increase in the system complexity.

Single-photon level.—Finally, to verify that these frequency mode mixers maintain performance at the single-photon level, we attenuate the input state $|\alpha_{\omega_0}(e^{-i\phi}\alpha)_{\omega_1}\rangle$ for the beam splitter and $|\alpha_{\omega_0}(e^{-i\phi}\alpha)_{\omega_1}(e^{-2i\phi}\alpha)_{\omega_2}\rangle$ for the tritter to ~ 0.1 photons per detection window at the gate input (i.e., before loss through the frequency mixer) and scan the input phase ϕ. The resulting interference patterns for these weak coherent states allow us to predict the operation fidelity for true single-photon states as well. This follows because the gate itself is a one-photon operation, and thus the interference visibility depends only on the average flux and any extra noise introduced by the gate—not on the photon number statistics of the input. At each setting, we use a wavelength-selective switch to direct the output modes to a gated InGaAs single-photon detector. Figure 5(a) plots the counts in modes 0 and 1 for the beam splitter, after subtracting the average detector dark count rate (error bars give the standard deviation of five repeated measurements). Moving on to the three-mode case, we obtain the detection rates for modes 0, 1, and 2 shown in Fig. 5(b). The oscillations now trace a sum of two sines, with respective peaks at $\phi = 0$, $2\pi/3$, and $4\pi/3$, as expected for the ideal matrix in Eq. (2). The reduced flux for mode 1 is primarily due to the wavelength-selective switch, as its 12.5-GHz passbands do not match the 18.1-GHz line spacing; in our filter definitions, the center of mode 1 is close to one passband edge and thereby experiences an additional ~ 1-dB attenuation. Overall, both the beam splitter and tritter perform exceptionally well at the single-photon level, with detector-dark-count-subtracted visibilities from 97% to 100%. Such low-flux visibilities far exceed those of previous $\chi^{(2)}$ or $\chi^{(3)}$
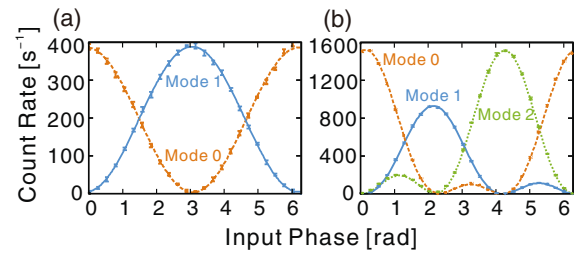

FIG. 4. Experimentally measured tritter output spectra for specific coherent-state inputs. (a) Pure mode 0, $|\alpha_{\omega_0}0_{\omega_1}0_{\omega_2}\rangle$. (b) Pure mode 1, $|0_{\omega_0}\alpha_{\omega_1}0_{\omega_2}\rangle$. (c) Pure mode 2, $|0_{\omega_0}0_{\omega_1}\alpha_{\omega_2}\rangle$. (d) Outputs for the superposition state input $|\alpha_{\omega_0}(e^{-i\phi}\alpha)_{\omega_1}(e^{-2i\phi}\alpha)_{\omega_2}\rangle$ for (I) $\phi = 0$, (II) $\phi = 2\pi/3$, and (III) $\phi = 4\pi/3$.

FIG. 5. Spectral interference with weak coherent states. (a) Output count rates for the two frequency modes of the beam splitter, as the phase ϕ of the single-photon-level state $|\alpha_{\omega_0}(e^{-i\phi}\alpha)_{\omega_1}\rangle$ is scanned. (b) Counts for the three output modes of the frequency tritter as the phase ϕ of the three-mode state $|\alpha_{\omega_0}(e^{-i\phi}\alpha)_{\omega_1}(e^{-2i\phi}\alpha)_{\omega_2}\rangle$ is scanned. The plotted best-fit curves are Fourier series of the form $\sum_n A_n \cos(n\phi + B_n)$, summed from $n = 0$ to 1 for (a) and $n = 0$ to 2 for (b).

frequency beam splitters, which suffer from optical noise generated by the powerful pump fields; our approach inherently contributes no excess noise photons, making it particularly well suited for quantum applications.

Discussion.—A major goal moving forward would be to fully integrate this frequency mixer, using on-chip modulators and pulse shapers—not only for reducing the overall footprint but also lowering the current ∼12.5-dB insertion loss, due primarily to our use of off-the-shelf telecommunication components. While our system's massive bandwidth could soften the impact of loss in the short term, through parallel replication of a desired operation, the ideal solution would be to reduce the loss altogether by improved engineering. An on-chip EOM with ∼1-dB loss has already been demonstrated [42], and an integrated pulse shaper with only ∼2-dB loss appears reasonable with established silicon-photonic processes [43]. Without a doubt, significant challenges remain to synthesize these capabilities onto a monolithic platform, demanding continued research and as-yet-uncharted technological advances. But the current state of the art nevertheless provides a legitimate promise for the development of high-throughput on-chip frequency gates, compatible with on-chip quantum frequency combs [44–48]. This integration would be extremely valuable, as the importance of electro-optic mixing has already been demonstrated in off-chip probing of the frequency entanglement of such frequency combs [47,48]. However, these examples used only one EOM and therefore suffered large amounts of scattering outside of the computational space [35]. By contrast, our multiple-EOM scheme permits inherently efficient true quantum gates—essential for the development of large-scale on-chip frequency QIP systems.

Finally, we note a useful connection between our electro-optic results and previous parametric beam splitters [7–11]. Since our technique excels for tightly spaced modes operated in parallel, whereas nonlinearity-based beam splitters instead perform well for interband modes spaced beyond typical electro-optic bandwidths, one can envision integrating *both* approaches in the same system: Computations can be performed in parallel within dense subbands with our technique, and the resulting photonic states can then be spectrally combined by parametric frequency mixers for further processing. In this way, the advantages of both approaches can be leveraged simultaneously, bringing us one step closer to the full utility of photonic QIP with frequency modes.

*lougovskip@ornl.gov

[1] J. Huang and P. Kumar, Phys. Rev. Lett. **68**, 2153 (1992).
[2] B. Brecht, A. Eckstein, A. Christ, H. Suche, and C. Silberhorn, New J. Phys. **13**, 065029 (2011).
[3] A. Eckstein, B. Brecht, and C. Silberhorn, Opt. Express **19**, 13770 (2011).
[4] B. Brecht, A. Eckstein, R. Ricken, V. Quiring, H. Suche, L. Sansoni, and C. Silberhorn, Phys. Rev. A **90**, 030302 (2014).
[5] P. Manurkar, N. Jain, M. Silver, Y.-P. Huang, C. Langrock, M. M. Fejer, P. Kumar, and G. S. Kanter, Optica **3**, 1300 (2016).
[6] V. Ansari, M. Allgaier, L. Sansoni, B. Brecht, J. Roslund, N. Treps, G. Harder, and C. Silberhorn, arXiv:1607.03001v1.
[7] T. Kobayashi, R. Ikuta, S. Yasui, S. Miki, T. Yamashita, H. Terai, T. Yamamoto, M. Koashi, and N. Imoto, Nat. Photonics **10**, 441 (2016).
[8] T. Kobayashi, D. Yamazaki, K. Matsuki, R. Ikuta, S. Miki, T. Yamashita, H. Terai, T. Yamamoto, M. Koashi, and N. Imoto, Opt. Express **25**, 12052 (2017).
[9] H. J. McGuinness, M. G. Raymer, C. J. McKinstrie, and S. Radic, Phys. Rev. Lett. **105**, 093604 (2010).
[10] S. Clemmen, A. Farsi, S. Ramelow, and A. L. Gaeta, Phys. Rev. Lett. **117**, 223601 (2016).
[11] C. Joshi, A. Farsi, and A. Gaeta, Hong-Ou-Mandel interference in the frequency domain, in *Proceedings of the Conference on Lasers and Electro-Optics* (Optical Society of America, Washington, DC, 2017), p. FF2E.3, https://www.osapublishing.org/abstract.cfm?uri=CLEO_QELS-2017-FF2E.3.
[12] J. M. Lukens and P. Lougovski, Optica **4**, 8 (2017).
[13] K. Azuma, K. Tamaki, and H.-K. Lo, Nat. Commun. **6**, 6787 (2015).
[14] M. Hillery, J. Bergou, and E. Feldman, Phys. Rev. A **68**, 032314 (2003).
[15] D. S. Simon, C. A. Fitzpatrick, S. Osawa, and A. V. Sergienko, Phys. Rev. A **95**, 042109 (2017).
[16] D. S. Simon, C. A. Fitzpatrick, and A. V. Sergienko, Phys. Rev. A **93**, 043845 (2016).
[17] L. Olislager, J. Cussey, A. T. Nguyen, P. Emplit, S. Massar, J.-M. Merolla, and K. P. Huy, Phys. Rev. A **82**, 013804 (2010).
[18] S. T. Cundiff and A. M. Weiner, Nat. Photonics **4**, 760 (2010).
[19] A. M. Weiner, Opt. Commun. **284**, 3669 (2011).
[20] A. Pe'er, B. Dayan, A. A. Friesem, and Y. Silberberg, Phys. Rev. Lett. **94**, 073601 (2005).
[21] F. Zäh, M. Halder, and T. Feurer, Opt. Express **16**, 16452 (2008).
[22] C. Bernhard, B. Bessire, T. Feurer, and A. Stefanov, Phys. Rev. A **88**, 032322 (2013).
[23] J. M. Lukens, A. Dezfooliyan, C. Langrock, M. M. Fejer, D. E. Leaird, and A. M. Weiner, Phys. Rev. Lett. **111**, 193603 (2013).
[24] J. M. Lukens, A. Dezfooliyan, C. Langrock, M. M. Fejer, D. E. Leaird, and A. M. Weiner, Phys. Rev. Lett. **112**, 133602 (2014).
[25] A. Agarwal, J. M. Dailey, P. Toliver, and N. A. Peters, Phys. Rev. X **4**, 041038 (2014).

[26] P. Kolchin, C. Belthangady, S. Du, G. Y. Yin, and S. E. Harris, Phys. Rev. Lett. **101,** 103601 (2008).

[27] C. Belthangady, C.-S. Chuu, I. A. Yu, G. Y. Yin, J. M. Kahn, and S. E. Harris, Phys. Rev. Lett. **104,** 223601 (2010).

[28] C. Liu, Y. Sun, L. Zhao, S. Zhang, M. M. T. Loy, and S. Du, Phys. Rev. Lett. **113,** 133601 (2014).

[29] M. Karpinski, M. Jachura, L. J. Wright, and B. J. Smith, Nat. Photonics **11,** 53 (2017).

[30] L. J. Wright, M. Karpiński, C. Söller, and B. J. Smith, Phys. Rev. Lett. **118,** 023601 (2017).

[31] S. E. Harris, Phys. Rev. A **78,** 021807 (2008).

[32] S. Sensarn, G. Y. Yin, and S. E. Harris, Phys. Rev. Lett. **103,** 163601 (2009).

[33] C. Belthangady, S. Du, C.-S. Chuu, G. Y. Yin, and S. E. Harris, Phys. Rev. A **80,** 031803 (2009).

[34] J. M. Lukens, O. D. Odele, D. E. Leaird, and A. M. Weiner, Opt. Lett. **40,** 5331 (2015).

[35] See Supplemental Material at http://link.aps.org/supplemental/10.1103/PhysRevLett.120.030502 for a discussion on the limits of a single EOM, information on the numerical optimization, details of the experimental methods, the multiport characterization procedure, and examples of measured matrices.

[36] D. B. Uskov, L. Kaplan, A. M. Smith, S. D. Huver, and J. P. Dowling, Phys. Rev. A **79,** 042326 (2009).

[37] S. Rahimi-Keshari, M. A. Broome, R. Fickler, A. Fedrizzi, T. C. Ralph, and A. G. White, Opt. Express **21,** 13450 (2013).

[38] A. Zeilinger, H. Bernstein, D. Greenberger, M. Horne, and M. Zukowski, in *Quantum Control and Measurement*, edited by H. Ezawa and Y. Murayama (Elsevier, New York, 1993), pp. 9–22.

[39] A. J. Menssen, A. E. Jones, B. J. Metcalf, M. C. Tichy, S. Barz, W. S. Kolthammer, and I. A. Walmsley, Phys. Rev. Lett. **118,** 153603 (2017).

[40] I. Agha, M. Davanço, B. Thurston, and K. Srinivasan, Opt. Lett. **37,** 2997 (2012).

[41] Higher frequencies could be obtained by using appropriate *V*-band (40–75 GHz) hardware.

[42] L. Fan, C.-L. Zou, M. Poot, R. Cheng, X. Guo, X. Han, and H. X. Tang, Nat. Photonics **10,** 766 (2016).

[43] AIM Photonics, http://www.aimphotonics.com/pdk/.

[44] D. Grassani, S. Azzini, M. Liscidini, M. Galli, M. J. Strain, M. Sorel, J. E. Sipe, and D. Bajoni, Optica **2,** 88 (2015).

[45] C. Reimer, M. Kues, P. Roztocki, B. Wetzel, F. Grazioso, B. E. Little, S. T. Chu, T. Johnston, Y. Bromberg, L. Caspani, D. J. Moss, and R. Morandotti, Science **351,** 1176 (2016).

[46] J. A. Jaramillo-Villegas, P. Imany, O. D. Odele, D. E. Leaird, Z.-Y. Ou, M. Qi, and A. M. Weiner, Optica **4,** 655 (2017).

[47] P. Imany, J. A. Jaramillo-Villegas, O. D. Odele, K. Han, M. Qi, D. E. Leaird, and A. Weiner, Demonstration of frequency-bin entanglement in an integrated optical microresonator, in *Proceedings of the Conference on Lasers and Electro-Optics* (Optical Society of America, Washington, DC, 2017), p. JTh5B.3, https://www.osapublishing.org/abstract.cfm?uri=CLEO_SI-2017-JTh5B.3.

[48] M. Kues, C. Reimer, P. Roztocki, L. R. Corts, S. Sciara, B. Wetzel, Y. Zhang, A. Cino, S. T. Chu, B. E. Little, D. J. Moss, L. Caspani, J. Azaña, and R. Morandotti, Nature (London) **546,** 622 (2017).